Applied Physics Letters

Two-dimensional high-quality Ag/Py magnetoplasmonic crystals

Cite as: Appl. Phys. Lett. **116**, 013106 (2020); https://doi.org/10.1063/1.5135711
Submitted: 08 November 2019 . Accepted: 23 December 2019 . Published Online: 10 January 2020

A. R. Pomozov, A. L. Chekhov, I. A. Rodionov, A. S. Baburin, E. S. Lotkov, M. P. Temiryazeva, K. N. Afanasyev, A. V. Baryshev, and T. V. Murzina

View Online Export Citation CrossMark

ARTICLES YOU MAY BE INTERESTED IN

Role of temperature-dependent electron trapping dynamics in the optically driven nanodomain transformation in a $PbTiO_3/SrTiO_3$ superlattice
Applied Physics Letters **116**, 012901 (2020); https://doi.org/10.1063/1.5128364

Detection of spin-orbit torque with spin rotation symmetry
Applied Physics Letters **116**, 012404 (2020); https://doi.org/10.1063/1.5129548

Selective ablation of cancer cells with low intensity pulsed ultrasound
Applied Physics Letters **116**, 013701 (2020); https://doi.org/10.1063/1.5128627

© 2020 Author(s).

AIP Publishing

Applied Physics Letters ARTICLE scitation.org/journal/apl

Two-dimensional high-quality Ag/Py magnetoplasmonic crystals

Cite as: Appl. Phys. Lett. **116**, 013106 (2020); doi: 10.1063/1.5135711
Submitted: 8 November 2019 · Accepted: 23 December 2019 ·
Published Online: 10 January 2020

View Online Export Citation CrossMark

A. R. Pomozov,[1] A. L. Chekhov,[1] I. A. Rodionov,[2,3] A. S. Baburin,[2,3] E. S. Lotkov,[2,3] M. P. Temiryazeva,[4] K. N. Afanasyev,[2,4] A. V. Baryshev,[2] and T. V. Murzina[1,a)]

AFFILIATIONS

[1]Department of Physics, M. V. Lomonosov Moscow State University, Moscow 119991, Russia
[2]Dukhov Automatics Research Institute, Federal State Unitary Enterprise, Moscow 127055, Russia
[3]FMN Laboratory, Bauman Moscow State Technical University, Moscow 105005, Russia
[4]Kotelnikov Institute of Radio Engineering and Electronics RAS, pl. Vvedenskogo, Fryazino, Moscow District 141190, Russia

[a)]Author to whom correspondence should be addressed: murzina@mail.ru

ABSTRACT

We demonstrate a perspective approach for the fabrication of functional high-quality magnetoplasmonic crystals based on a 2D periodical perforated silver film covered by a thin layer of ferromagnetic metal (Permalloy). The wavelength-angular spectra of the 2D crystals reveal a large number of high-quality resonant features associated with the excitation of surface plasmon-polariton modes of various orders. Due to the presence of a ferromagnetic material on both plasmonic interfaces, pronounced magnetic effects are observed for all excitations and are influenced by the coupling between various modes. The suggested magnetoplasmonic crystal composition with high-quality resonant optical and magneto-optical properties gives perspective for the control over the light propagation as well as for sensor applications.

Published under license by AIP Publishing. https://doi.org/10.1063/1.5135711

Magnetoplasmonic crystals (MPCs) that support the excitation of surface plasmon-polaritons (SPPs) with the possibility of the control of their spectral features by the external magnetic field attract a lot of interest, mostly from the point of view of their possible application as functional elements of photonics and plasmonics.[1,2] The most studied types of MPCs are either a nanostructured metal film, typically gold, placed on top of a magnetic dielectric,[3,4] or spatially periodic structures made of a ferromagnetic metal.[5,6] Depending on their composition, MPCs can reveal resonant SPP excitations that correspond to the phase-matching conditions. Moreover, due to the possibility of magnetic field control over their dispersion, the spectral position of the resonances can be modified, which leads to the appearance of the resonant amplification of the magneto-optical (MO) effects, as was demonstrated for different orientations of the magnetic field with respect to the plasmonic surface.[1–7]

It was also recognized that the magnitude of the MO effects depends drastically on the quality factors of the SPP resonances,[7] and so new approaches for the MPC composition providing a high quality factor of the MO resonances are very desired. It is well known that silver is the most effective plasmonic metal for the visible spectral range,[8–13] which can provide the highest values of the SPP quality factor. So the development of a magnetic plasmonic structure based on silver structures is a straightforward broadening of the class of plasmonic structures. In this Letter, we describe functional high-quality magnetoplasmonic crystals based on a 2D periodical perforated silver film coated by a thin Permalloy layer (Py).

2D Ag/Py ($Ni_{80}Fe_{20}$) MPCs are made by electron beam lithography as 2D arrays of holes in a 100 nm thick e-beam evaporated silver layer on a fused quartz substrate. The holes of 200 nm in diameter are ordered in a square lattice with a period of 545 nm, which allows for the observation of the SPP in the visible spectral range, the sample size being 500 μm × 500 μm. The SEM image of the sample is shown in Fig. 1(a). This structure is covered by a 10 nm-thick Permalloy layer [Fig. 1(a), inset]. A small mass thickness of the deposited Py was necessary to avoid the total filling of holes by the ferromagnetic metal. This can be seen in Fig. 1(b) that shows the AFM image of the resulting Ag/Py structure observed by SmartSPM (AIST-NT), which shows a good 2D periodicity of holes. The magnetic force microscopy image of the same area on the Ag/Py sample as in Fig. 1(d) was taken by NT-MDT NTEGRA Spectra [see Fig. 1(c)]. It shows that the whole structure including the inner part of the holes reveals the magnetic response, which confirms that Permalloy conformly covers the perforated film. So the structure exhibits two nonequivalent periodically modulated interfaces containing magnetic components, the upper one

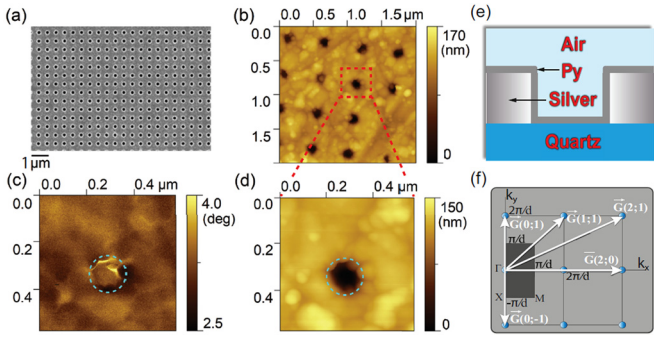

FIG. 1. (a) SEM image of the top-view of the 2D silver structure; (b) AFM image of the perforated 2D Ag/Py MPC; (c) MFM image of a single hole in 2D Ag/Py MPC; (d) enlarged AFM image of the area shown in (b). Schematic view (e) of the cross section of the 2D Ag/Py MPC and (f) of a square reciprocal lattice; white arrows show possible reciprocal lattice vectors; the dark gray rectangle denotes the first Brillouin zone.

consisting of Ag/Py and air-filled spacings and quartz/Ag with quartz/Py spacings, which should provide extra resonant MO features as compared to previously studied MPC. Further, for the sake of simplicity, the upper interface of the structure, Ag/air or Py + Ag/air, will be denoted as 1 and the bottom one, Ag/quartz or Py + Ag/quartz, as 2.

Optical experiments are performed in transmission geometry, and the angle of incidence of the p- or s-polarized probe beam was varied from -5° up to 50° by 0.5° increments. A halogen lamp was used as the light source; radiation was collimated and focused to a spot of 300 μm in diameter, the plane of incidence being parallel to the edge of the surface grating. The transmitted radiation was analyzed using an Avesta ASP-75 spectrometer, which provided a spectral resolution of 1–1.5 nm in the spectral range of 400–1000 nm. Magneto-optical experiments were performed in transmission through the MPC, and the angle of incidence of the p-polarized probe beam was varied from -10° up to 40° by 0.5° increments. Magnetic field induced modulation of the intensity of the transmitted radiation was registered in the Voigt geometry and characterized by the magneto-optical contrast $\rho = [T(M) - T(-M)]/[T(M) + T(-M)]$, where $T(M)$ and $T(-M)$ are the values of the transmission measured for the opposite directions of the external magnetic field of 1.5 Oe.

Figures 2(a) and 2(b) show the experimental wavelength-angular transmission spectra of the as-prepared 2D Ag structure for the s- and p-polarized incident light. It reveals a number of high-quality resonant features. We performed the analysis of these spectra by calculating the SPP excitation conditions based on the momentum conservation equation, which, for a 2D plasmonic crystal, takes the following form:

$$\vec{k}_{spp} = \vec{k}_x \pm n\vec{G}_x \pm m\vec{G}_y = \frac{2\pi}{\lambda}\sqrt{\frac{\varepsilon_{Ag}\varepsilon_d}{\varepsilon_{Ag}+\varepsilon_d}}, \quad (1)$$

where $\vec{k}_{spp}$ is the SPP wave vector, $k_x = (2\pi/\lambda)\sin\theta$ is the in-plane component of the wave vector of the incident light, θ is the angle of incidence, λ is the wavelength of light in vacuum, $(n, m) \in Z$, and $|\vec{G}_x| = |\vec{G}_y| = \frac{2\pi}{d}$ are the reciprocal lattice vectors for a 2D square lattice with the period d; ε_{Ag} and ε_d are the dielectric constants of silver and a dielectric (air or fused quartz). Thus, the dispersion curves on the wavelength-angular plots are described by the following function:

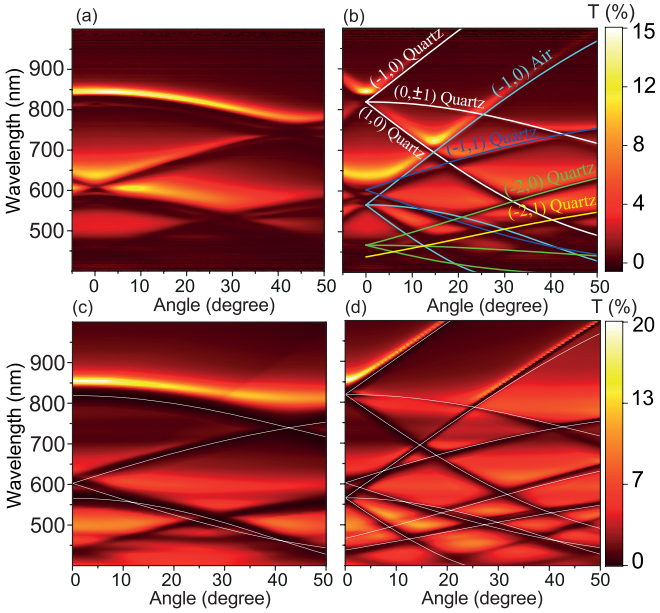

FIG. 2. Angle- and polarization-resolved transmission spectra of the 2D Ag plasmonic crystal measured for the s-polarized (a) and p-polarized (b) probe beams. Dispersion of surface plasmons shows solid curves (b). Numerically calculated angle- and polarization-resolved transmission spectra of the 2D Ag plasmonic crystal with dispersion curves for the s-polarized (c) and p-polarized (d) probe beam by the FDTD method.

$$\frac{1}{\lambda^2}\left|\frac{\varepsilon_{Ag}\varepsilon_d}{\varepsilon_{Ag}+\varepsilon_d}\right| = \left(\frac{\sin\theta}{\lambda}+\frac{n}{d}\right)^2 + \left(\frac{m}{d}\right)^2. \quad (2)$$

The corresponding calculated dispersion curves for a 2D Ag-based plasmonic crystal are shown in Figs. 2(c) and 2(d) by lines, and the pair of numbers (n, m) noted nearby corresponds to those used for the calculation of the SPP dispersion described by Eq. (2). It can be seen that the SPP excitations with the modes' numbers n, m = (0, 1, 2) correspond to the minima in the transmission spectra, which are consistent with the results reported previously for other types of plasmonic crystals. The Q-factor for the resonant SPP modes of 10^2 reveals expected low losses of the silver structure; along with high steepness of the slope, it is quite attractive for sensor applications. Different slopes of the resonant dependencies shown in Fig. 2 refer to different SPP modes excited in the structure. The largest slope corresponds to the SPP propagating along the X axis at interfaces 1 and 2, i.e., to the $(\pm 1; 0)$ modes. The fine structure and properties of these modes are discussed below.

To analyze these data, we calculated the transmission spectra of the Ag-based plasmonic crystals using the FDTD method (Lumerical Solutions) as shown in Figs. 2(c) and 2(d). The simulation was made by using a plane wave source with the angular step of 0.5° and the wavelength step of 5 nm. One can see good agreement between the theoretical and experimental spectra, including the whole diversity of higher-order plasmon modes, which confirms that the observed spectral minima in the transmission are attributed to the SPP excitation.

Analogous measurements were carried out for the 2D Ag/Py MPC. Figures 3(a) and 3(b) show the wavelength-angular spectra of

Published under license by AIP Publishing

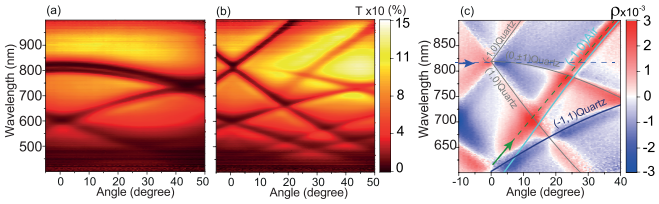

FIG. 3. (a) and (b) Wavelength-angular transmission spectra of Ag/Py MPC for the s- and p-polarized probe beams. (c) Wavelength-angular spectra of the magneto-optical contrast measured in transmission through the Ag/Py MPC in the Voigt geometry for the p-polarized probe beam. SPP dispersion curves calculated for the considered samples using Eq. (2) (solid and dashed lines), the modes' numbers are noted nearby.

this structure measured for the s- and p-polarizations of the fundamental beam. It can be seen that deposition of a 10 nm thick Permalloy layer decreases the average transmission by nearly an order of magnitude and thus reduces the Q-factor of the SPP resonances down to approximately 15. This is caused by high losses introduced by the Py film. Nevertheless, the spectra of the SPP resonances remained unchanged, which show that the silver structure is dominant in the formation of SPP resonance features.

Figure 3(c) shows the spectrum of the magneto-optical contrast, ρ, measured in the Voigt geometry for the p-polarized incident radiation, positive and negative ρ values correspond to blue and red colors, and the SPP modes' are shown along with their numbers. One can see that close to the SPP modes specific to the two plasmonic interfaces, a strong modulation of the MO effect takes place, the changes of the ρ sign and its maxima being observed in the vicinity of these modes. At the same time, in general, the ρ value is larger for interface 1 as compared to the 2 one, which is consistent with different surface densities of Permalloy at these interfaces. The maximal value of the MO contrast associated with the SPP curves is about $2 \div 3 \times 10^{-3}$, which exceeds the value of the effect for a continuous Ag/Py film of similar mass thickness. Another issue to be pointed out is a pronounced asymmetry of the ρ spectra, which is an attribute of the Fano-type resonance, which will be discussed below.

Let us consider in more detail the most interesting features of optical transmission spectra shown in Figs. 2 and 3. First, pronounced asymmetry of the transmission spectra is typical for plasmonic structures and can be described by Fano-type resonances, as the transmitted electromagnetic field contains two coherent components, a resonant one that experiences a strong amplitude and phase modulation near the SPP excitation at interface 1 or 2 and a nonresonant one, which corresponds to all other transmitted waves. The resultant outgoing field is determined by the interference of these two terms, similar to that discussed for other types of plasmonic structures.[14–16] This asymmetry can be seen in more detail in Fig. 4(a), which shows the spectral dependencies of the transmission for the two angles of incidence, $\theta = 0°$ and $\theta = 15°$. Besides, in the absence of the Py layer, the 2D Ag plasmonic crystal at normal incidence reveals the so-called anomalous transmission, where the value of the normalized transmission $T_N = T(\lambda, \theta)/T_{eff}$ is approximately 143% for the transmission maximum at $\theta = 15\%$ and $\lambda = 850$ nm [Fig. 4(a)]. Here, the effective transmission T_{eff} is determined as the fraction of the area occupied by the holes and is 10.5%, while the continuous Ag film is nontransparent. Among various possible mechanisms of the anomalous transmission in thin perforated films, such as the interaction of plasmons excited at two interfaces,[17–19] the so-called Woods' anomaly,[20] the interaction of plasmons with eigenmodes of the holes in the metal[21] seems the most reliable in our case.

A larger number of SPP modes for the p-polarized probe beam as compared to those for the s-polarization is typical for 2D plasmonic crystals, as in that case different projections of the $\mathbf{k}_x$ vector participate in the SPP momentum conservation described by Eq. (2).

At the same time, the high quality of the plasmon resonances for the s-polarized probe beam allows us to distinguish the fine structure of one of the most pronounced SPP modes $(0; \pm 1)$ propagating at interface 2. One can see a clear splitting of this mode into two at oblique incidence and a doublet peak at normal incidence. This effect can be explained when considering the dark SPP modes, which possess a zero average dipole moment and a nonzero quadrupole one.[22]

Magneto-optical effects in MPC appear due to the magnetic field induced spectral shift of the SPP dispersion curves according to the modified dispersion equation, which takes the following form for the Voigt geometry:[23]

$$k_{spp} = \frac{2\pi}{\lambda}\sqrt{\frac{\varepsilon_{Ag}\varepsilon_d}{\varepsilon_{Ag}+\varepsilon_d}}(1 \pm \alpha g), \tag{3}$$

where $g \propto M$ (M—magnetization of the medium) is the gyration vector and $\alpha = (-\varepsilon_{Ag}\varepsilon_d)^{-1/2}(1 - \varepsilon_d^2/\varepsilon_{Ag}^2)^{-1}$.

Thus, depending on the direction of the SPP propagation, magneto-optical contrast has the opposite signs and vanishes at

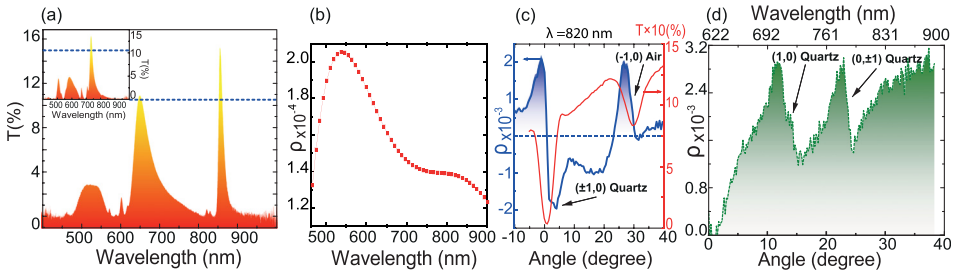

FIG. 4. (a) Sections from Fig. 2(b). Transmission spectra of the 2D Ag plasmonic crystal for the p-polarized probe beam at normal (main) and $\theta = 15°$ (inset) angles of incidence. Blue dashed lines indicate the fraction of the area occupied by the holes. (b) MO contrast for the Permalloy thin film of 10 nm thickness for the probe beam with an incidence angle of 40°. (c) and (d) Sections from Fig. 3(c): (c) the MO contrast-angular dependence at the wavelength of 820 nm (blue line) and transmission (red line). (d) MO contrast section along the plasmon mode (−1, 0) Air (green dashed line).

Published under license by AIP Publishing

normal incidence, where the counter propagating SPPs at plasmonic interfaces compensate each other; this is confirmed by the experimental data. In the region of intersection of plasmon dispersions for two interfaces, the magneto-optical contrast is additively added and its value increases. We would like to emphasize that the angular spectrum of the MO contrast reveals quite sharp drops, as can be seen in Fig. 4(c). Here, the angular spectrum of ρ is shown for the wavelength of 820 nm. It can be seen that in the vicinity of $\theta = 0°$, the magneto-optical contrast changes by the value of 4×10^{-3} as the angle of incidence is varied for 1°–2°. Such a sharp drop is rather perspective for sensor applications.

Figure 4(c) illustrates the angular dependence of the magnitude of MO contrast due to plasmon excitation at interface 2, when the probing light had the wavelength of 820 nm. To understand the observed features, the following should be taken into account. As seen from Fig. 4(a), the so-called dark modes, also known as the high-Q modes,[24–26] manifest themselves as a double peak in the vicinity of 820 nm. These modes were visualized because the probing light beam was focused, and the (−1, 0) and (1, 0) SPP modes were split apart at normal incidence. Next, Permalloy deposited on the surface of the perforated film was likely deposited into the holes of the considered 2D nanostructure, which means that the holes themselves became magnetic ones. Finally, the spectral features in the range of the Rayleigh-Wood anomaly are defined by the interference of exited modes[27]—in our case, the SPP mode due to the plasmon on interface 2 and the localized modes of magnetic holes. This was why, though most of Permalloy was deposited on interface 1, the considered 2D nanostructure exhibited the MO contrast with the values of similar magnitude as those in Fig. 4(d) for interface 1.

In summary, we have developed and studied a perspective type of magnetoplasmonic crystal based on a two-dimensional periodic perforated silver film of the thickness of 100 nm coated with a 10 nm layer of Permalloy. Transmission spectra of the pure Ag 2D plasmonic crystals and those covered by Py show resonant excitation of a number of surface plasmon-polariton modes satisfying the phase-matching conditions. The linear transverse magneto-optical effect shows that the presence of the Permalloy layer that covers conformly the perforated Ag film provides a magnetic response at the two interfaces. At the intersection of plasmon dispersion for two interfaces, drastic changes in the magneto-optical response are attained including the change of sign of the magneto-optical contrast that reaches the values up to 3×10^{-3}. This is an order of magnitude higher than the magneto-optical effect of a single Permalloy film thickness of similar thickness [Fig. 4(b)].

This work was partially supported by the Russian Foundation for Basic Research, Grant No. 19-02-00826. A.R.P. also acknowledges the financial support from the Foundation for the advancement of theoretical physics and mathematics (BASIS). Samples were made at the BMSTU Nanofabrication Facility (Functional Micro/Nanosystems, FMNS REC, ID 74300). The authors acknowledge useful discussions with A. N. Shaimanov.

REFERENCES

[1]G. Armelles, A. Cebollada, A. Garcia-Martin, and M. U. Gonzalez, Adv. Opt. Mater. **1**, 10 (2013).
[2]G. A. Wurtz, W. Hendren, R. Pollard, R. Atkinson, L. Le Guyader, A. Kirilyuk, Th. Rasing, I. I. Smolyaninov, and A. V. Zayats, New J. Phys. **10**, 105012 (2008).
[3]V. I. Belotelov, I. A. Akimov, M. Pohl, V. A. Kotov, S. Kasture, A. S. Vengurlekar, A. V. Gopal, D. Yakovlev, A. K. Zvezdin, and M. Bayer, Nat. Nanotechnol. **6**, 370 (2011).
[4]A. L. Chekhov, V. L. Krutyanskiy, V. A. Ketsko, A. I. Stognij, and T. V. Murzina, Opt. Mater. Express **5**, 1647 (2015).
[5]A. V. Chetvertukhin, A. A. Grunin, A. V. Baryshev, T. V. Dolgova, H. Uchida, M. Inoue, and A. A. Fedyanin, J. Magn. Magn. Mater. **324**, 3516 (2012).
[6]N. Maccaferri, M. Kataja, V. Bonanni, S. Bonetti, Z. Pirzadeh, A. Dmitriev, S. van Dijken, J. Akerman, and P. Vavassori, Phys. Status Solidi A **211**, 1067 (2014).
[7]N. Bonod, R. Reinisch, E. Popov, and M. Neviere, J. Opt. Soc. Am. B **21**, 791 (2004).
[8]K. S. Lee and M. A. El-Sayed, J. Phys. Chem. B **110**, 19220 (2006).
[9]P. Tassin, T. Koschny, M. Kafesaki, and C. M. Soukoulis, Nat. Photonics **6**, 259 (2012).
[10]A. Boltasseva and H. A. Atwater, Science **331**, 290 (2011).
[11]A. S. Baburin, A. M. Merzlikin, A. V. Baryshev, I. A. Ryzhikov, Y. V. Panfilov, and I. A. Rodionov, Opt. Mater. Express **9**, 611 (2019).
[12]A. S. Baburin, A. S. Kalmykov, R. V. Kirtaev, D. V. Negrov, D. O. Moskalev, I. A. Ryzhikov, P. N. Melentiev, I. A. Rodionov, and V. I. Balykin, Opt. Mater. Express **8**, 3254 (2018).
[13]I. A. Rodionov, A. S. Baburin, A. R. Gabidullin, S. S. Maklakov, S. Peters, I. A. Ryzhikov, and A. V. Andriyash, Sci. Rep. **9**(1), 12232 (2019).
[14]K. L. Lee, C. C. Chang, M. L. You, M. Y. Pan, and P. K. Wei, Sci. Rep. **6**, 33126 (2016).
[15]H. F. Ghaemi, T. Thio, D. E. Grupp, T. W. Ebbesen, and H. J. Lezec, Phys. Rev. B **58**, 6779 (1998).
[16]L. Martin-Moreno, F. J. Garcia-Vidal, H. J. Lezec, K. M. Pellerin, T. Thio, J. B. Pendry, and T. W. Ebbesen, Phys. Rev. Lett. **86**, 1114 (2001).
[17]T. Thio, H. F. Ghaemi, H. J. Lezec, P. A. Wolff, and T. W. Ebbesen, J. Opt. Soc. Am. B **16**, 1743 (1999).
[18]R. Nicolas, G. Leveque, J. Marae-Djouda, G. Montay, Y. Madi, J. Plain, Z. Herro, M. Kazan, P.-M. Adam, and Th. Maurer, Sci. Rep. **5**, 14419 (2015).
[19]C. Genet, M. P. van Exter, and J. P. Woerdman, Opt. Commun. **225**, 331 (2003).
[20]A. Hessel and A. A. Oliner, Appl. Opt. **4**, 1275 (1965).
[21]J. Parsons, I. R. Hooper, W. L. Barnes, and J. R. Sambles, J. Mod. Opt. **56**, 1199 (2009).
[22]A. A. Yanik, A. E. Cetin, M. Huang, A. Artar, S. H. Mousavi, A. Khanikaev, J. H. Connor, G. Shvets, and H. Altug, Proc. Natl. Acad. Sci. U. S. A. **108**, 11784 (2011).
[23]V. I. Belotelov, L. E. Kreilkamp, I. A. Akimov, A. N. Kalish, D. A. Bykov, S. Kasture, V. J. Yallapragada, A. V. Gopa, A. M. Grishin, S. I. Khartsev *et al.*, Nat. Commun. **4**, 2128 (2013).
[24]A. K. Zvezdin and V. A. Kotov, *Modern Magnetooptics and Magnetooptical Materials*, 1st ed. (CRC Press, 1997), ISBN 9780750303620.
[25]V. T. Tenner, A. N. van Delft, M. J. A. de Dood, and M. P. van Exter, J. Opt. **16**, 114019 (2014).
[26]M. P. Van Exter, V. T. Tenner, F. van Beijnum, M. J. A. de Dood, P. J. van Veldhoven, and E. J. Geluk, Opt. Express **21**, 27422 (2013).
[27]A. N. Shaimanov, N. A. Orlikovsky, E. M. Khabushev, A. V. Zverev, A. A. Pishimova, G. V. Sharonov, G. M. Yankovskii, I. A. Rodionov, and A. V. Baryshev, Photonics Nanostruct. Fundam. Appl. **32**, 1 (2018).

Published under license by AIP Publishing